Nanoscale

RSC Publishing

PAPER

View Article Online
View Journal | View Issue

Cite this: *Nanoscale*, 2013, **5**, 1159

In situ detection of dopamine using nitrogen incorporated diamond nanowire electrode†

Jayakumar Shalini,[a] Kamatchi Jothiramalingam Sankaran,[a] Chung-Li Dong,[b] Chi-Young Lee,*[a] Nyan-Hwa Tai[a] and I-Nan Lin*[c]

Received 27th September 2012
Accepted 26th November 2012

DOI: 10.1039/c2nr32939e

www.rsc.org/nanoscale

Significant difference was observed for the simultaneous detection of dopamine (DA), ascorbic acid (AA), and uric acid (UA) mixture using nitrogen incorporated diamond nanowire (DNW) film electrodes grown by microwave plasma enhanced chemical vapor deposition. For the simultaneous sensing of ternary mixtures of DA, AA, and UA, well-separated voltammetric peaks are obtained using DNW film electrodes in differential pulse voltammetry (DPV) measurements. Remarkable signals in cyclic voltammetry responses to DA, AA and UA (three well defined voltammetric peaks at potentials around 235, 30, 367 mV for DA, AA and UA respectively) and prominent enhancement of the voltammetric sensitivity are observed at the DNW electrodes. In comparison to the DPV results of graphite, glassy carbon and boron doped diamond electrodes, the high electrochemical potential difference is achieved *via* the use of the DNW film electrodes which is essential for distinguishing the aforementioned analytes. The enhancement in EC properties is accounted for by increase in sp^2 content, new C–N bonds at the diamond grains, and increase in the electrical conductivity at the grain boundary, as revealed by X-ray photoelectron spectroscopy and near edge X-ray absorption fine structure measurements. Consequently, the DNW film electrodes provide a clear and efficient way for the selective detection of DA in the presence of AA and UA.

Introduction

Electrochemical (EC) detection of dopamine (DA) has received intense attention for the last few decades to investigate the role of neurotransmitters in the brain due to their electroactive nature.[1] Dopamine is a key neurotransmitter molecule of catecholamines in mammalian central and peripheral nervous systems.[2,3] It plays a vital role in the functioning of central nervous, renal, hormonal and cardiovascular systems. However, its deficiency will lead to brain disorder such as Parkinson's disease[4] and schizophrenia.[5] Therefore, it is the clinical significance to develop clear and effective method for measuring DA to prevent these diseases. EC determination of DA has demonstrated to be a preferred method due to its simplicity, fast response, and high sensitivity.[6–12] However, a major problem facing the EC detection of DA is serious interferences caused by the coexisting substances, such as AA and UA.[13–15] Because the EC oxidation peak potentials for AA, DA, and UA are similar, the conventional electrodes suffer from fouling by the oxidation products, which results in reduced selectivity and reproducibility.[13,16,17] Additionally, the oxidation of DA at the electrode surface may also result in a homogeneous catalytic oxidation of AA and UA. To overcome such limitations, various chemically modified electrodes such as metal complexes or nanoparticles,[18–21] organic redox mediators,[22,23] polymers[24–26] and carbon-based materials[27–34] have been demonstrated since

[a]*Department of Material Science and Engineering, National Tsing-Hua University, Hsinchu 300, Taiwan, R.O.C. E-mail: cylee@mx.nthu.edu.tw; inanlin@mail.tku.edu.tw*

[b]*Scientific Research Division, National Synchrotron Radiation Research Center, Hsinchu 300, Taiwan, R.O.C*

[c]*Department of Physics, Tamkang University, New-Taipei 251, Taiwan, R.O.C*

† Electronic supplementary information (ESI) available: Additional figure including cyclic voltammetric curve for the DNW film electrodes at different T_S using (a) 0.1 mM $Fe(CN)_6^{3-/4-}$, (b) 0.1 mM $Ru(NH_3)_6^{2+/3+}$ and (c) 0.1 mM 4-*tert*-butylcatechol in 0.1 M KCl (Fig. S1), differential pulse voltammetry curve for graphite, glassy carbon and boron doped diamond electrodes in a solution containing 0.33 mM AA + 0.033 mM DA + 0.033 mM UA (Fig. S2). Differential pulse voltammetry curves for diamond nanowire and boron doped diamond electrodes in a solution containing 0.33 mM AA + 0.033 mM DA + 0.033 mM UA (Fig. S3). Differential pulse voltammetry curves for fresh and prolonged usage of (a) diamond nanowire and (b) boron doped diamond electrode in a solution containing 0.33 mM AA + 0.033 mM DA + 0.033 mM UA (Fig. S4). Table S1 for oxidation peak currents of DNW film (700 °C) electrode shown in Fig. 5. Table S2 for dynamic range and limit of detection of DA in the presence of interference (AA and UA) obtained by differential pulse voltammetry using DNW film (700 °C) electrode. Comparison Table S3 for DNW film (700 °C) electrode with previously published results for the detection of AA, UA and DA using cyclic voltammetry with different electrodes. Comparison Table S4 for DNW film (700 °C) electrode with previously published results for the detection of DA using amperometric measurements with different electrodes. See DOI: 10.1039/c2nr32939e

the modified electrode can reduce the oxidation potential and also increase sensitivity, thus improving selectivity.[35]

In recent years, biosensors based on diamond have attracted immense attention as diamond is known to be biocompatible and chemically inert, and also shows excellent EC properties and long-term chemical stability of biomolecules bonded to it. Precisely, diamond film electrode grown by a chemical vapor deposition process possesses enhanced EC properties to be the focus of a wide range of applications.[36–38] These diamond film electrodes are synthesized by using either nitrogen or boron source, possess a high surface to volume ratio with significant π-bonding and sp^2 hybridization[39–41] resulting in high electrical conducting behavior with distinct EC properties.[42,43] Particularly, boron doped diamond (BDD) electrodes have been widely employed for the construction of various EC biosensors due to their remarkable properties, including a wide EC potential window, low and stable capacitive background current, high response reproducibility and good biocompatibility.[44–47] Besides, they have also been successfully applied to the EC sensing of AA, DA, and UA. For instance, the research group of Fujishima described the EC detection of DA in the presence of AA at BDD (hydrogen terminated and oxygen-terminated) electrodes.[48,49] Popa reported the selective detection of UA in the presence of AA at anodized BDD electrodes.[50] Zhi and Zhou also disclosed the functionalization of nanocrystalline BDD films *via* a photochemical reaction with undecylenic acid methyl ester and subsequent removal of the protection ester groups to produce a carboxyl-terminated surface for the detection of DA in the presence of AA.[51,52] Recently, Weng *et al.* also described an EC performance of DA and AA on the Au/BDD electrode.[53] Besides these reports, EC oxidation of purine bases, adenine or guanine, and DNA has also been investigated using a surface modified BDD electrode.[54–57] Despite these significant developments, the BDD electrode surface modification needs to be delicately controlled and selectivity is still not satisfying enough. Thus, it would be highly noteworthy to look for efficient as well as convenient non-surface modified new electrode materials for the simultaneous detection of DA, AA and UA.

Recently, N_2-incorporation in growth plasma results in extreme modification in the properties of diamond materials. Incorporation of N_2 in the growth plasma leads to increase in the amorphous phase which in turn converts to a graphitic phase on annealing, defects contributing to the sp^2 at the grain boundaries, an increase in the overall grain boundary volume with increase in the density of states at the Fermi level.[58–60] Changes in the morphology of the electrodes with changes in different electrode deposition parameters can alter the properties of the structural properties, electrical conductivity, *etc.*, in the material.[61–64] The changes in the dimensions of the nanowires formed were reported by Arenal *et al.*, where sp^2 content increased and also covered the sp^3 diamond phase in the wires,[65] whereas Sobia *et al.* demonstrated that a change in N_2 concentration does not play a role in defining the wire-like growth of diamond grains in their studies.[66,67] Teii and Ikeda recorded a change in the morphology, thereby analyzed the increase in graphitic content with improved sp^2 bond angle order for trivalent carbon atoms in addition to C–N bonds, with increase of the substrate temperature (T_S).[68] On the other hand, N_2-incorporated diamond film electrodes were hardly demonstrated as EC electrodes to detect DA without electrode surface modification. Recently, Kang used as-grown N_2-incorporated nanodiamond electrodes to sense only DA.[69–71] In fact, to the best of our knowledge the simultaneous detection of DA, UA and AA based on N_2-incorporated diamond electrodes has not been reported yet. Herein, we report for the first time the simultaneous detection of DA, AA and UA using N_2-incorporated diamond nanowire (DNW) film electrodes without any surface modification such as addition of an electron transfer mediator or specific reagents using a differential pulse voltammetry (DPV) technique. The electronic structure of DNW films was elucidated by near edge X-ray absorption fine structure spectroscopy (NEXAFS) and X-ray photoelectron spectroscopy (XPS), to examine the various microstructural phases that altered the EC behavior of the DNW film electrodes.

Experiments

DNW films were grown on planar Si substrates using a microwave plasma enhanced chemical vapor deposition (MPECVD) method. Prior to the deposition, the substrates were ultrasonicated in methanol solution, containing nano-diamond powder ($\sim$5.0 nm) and titanium powder ($\sim$37.0 mesh), for 45 min to create nucleation sites. The DNW films were grown under different T_S using 6% CH_4/94% N_2 gas at 1200 W and 120 T for 30 min. Field emission scanning electron microscopy (FESEM, JEOL JSM 6500F) was used to characterize the surface morphologies of the DNW films. NEXAFS and XPS studies were used to analyze the electronic structure of the films. Hall measurements (ECOPIA) were carried out in a van der Pauw configuration to measure the electrical conductivity of the films.

The EC properties of the films were characterized using cyclic voltammetry (C-V, Autolab PGSTAT302, Netherlands). These measurements were made with CS-1087 computer-controlled potentiostat (C-V Autolab PGSTAT302, Netherlands). A standard three-electrode cell was employed. DNW films grown using T_S were used as working electrode (working area of 0.186 cm^2). A platinum (Pt) rod and silver/silver chloride (Ag/AgCl) electrodes served as the counter and reference electrodes. All potentials in this study are reported with respect to the Ag/AgCl electrode. All measurements were made at room temperature in a 0.1 M phosphate buffer solution (PBS) with pH 7.4. De-ionized water was used throughout the experiment. Buffer solution (PBS, pH 7.4) was prepared from NaH_2PO_4–Na_2HPO_4, dopamine hydrochloride, ascorbic acid, uric acid, potassium ferrocyanide, hexaminerutheniumIII chloride, 4-*tert*-butylcatechol. These chemicals were purchased from Aldrich chemicals which are reagent-grade quality, used without further purification. All solutions containing redox-active solutes were prepared freshly.

Results and discussion

Fig. 1 shows FESEM images of the densely packed DNWs films grown at different T_S in the same MPECVD system. The films

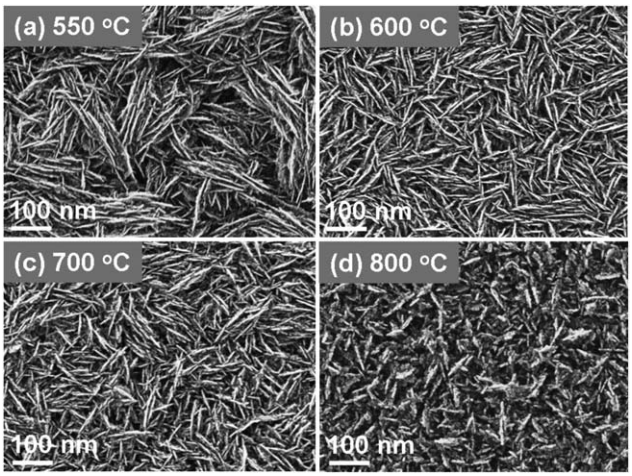

Fig. 1 FESEM images of diamond nanowire films grown at 550–800 °C.

grown from T_S = 550 to 700 °C show an uniform pattern of DNWs possessing a characteristic 'acicular' like structure in a few nanometers' width. For $T_S \geq 750$ °C, the acicular grains become larger in the lateral dimension, while the boundaries defining each grain become indistinguishable. The T_S dependent morphological changes of the films reflect in the electrical conducting behavior of the DNWs films, which is measured by van der Pauw Hall measurement method. The electrical conductivity of DNWs films first increases monotonously with increasing T_S, from 1.2 $(\Omega\ cm)^{-1}$ (carrier concentration of 5.8×10^{13} cm^{-2}) for DNWs films grown at T_S = 550 °C to about 186 $(\Omega\ cm)^{-1}$ with a carrier concentration of 2×10^{22} cm^{-2} for DNWs films with T_S = 700 °C. But the conductivity reverts to lower values for films grown at T_S > 700 °C, which is shown in Table 2. As a result, the films grown under 700 °C possess the highest electrical conductivity among other DNWs films.

To understand the change in electrical conductivity of the films grown at different T_S, a detailed investigation on the microstructural phases is carried out using NEXAFS and XPS. Fig. 2 shows the NEXAFS spectra of the films clearly ascertaining that the major part of the carbon is the sp^3 diamond phase with a smaller amount of sp^2 graphitic phase distributed in the films. The small peak at ~285 eV (ref. 72–75) is assigned to the C (1s)–π* transition corresponding to the sp^2 graphitic phase. A sharp peak at ~289 eV corresponds to the diamond electron core excitation of C–C (1s)–σ*, *i.e.*, the sp^3 diamond phase. A weak dip observed at ~302 eV (ref. 76–78) is assigned to the second

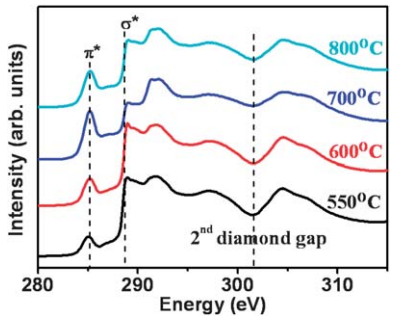

Fig. 2 NEXAFS spectra of diamond nanowire films grown at 550–800 °C.

absorption band gap of the diamond. The magnified image of the peak at ~285 eV (figure not shown) with the maximum intensity for the films grown at T_S = 700 °C confirms that these films possess a high sp^2 graphitic phase which results in high electrical conductivity.

Furthermore, XPS studies were carried out to investigate in detail the chemical bonding of the DNW films. C 1s peak has successfully been adopted to estimate the sp^3 content in DNW films grown at different T_S. The XPS spectra of the DNW films obtained in this study were performed using the Al Kα-line. The measurement was conducted without ion sputtering etching, to avoid reconfiguration of the bonds. The C 1s spectra of the DNW films clearly show that the spectral line shape of the DNW

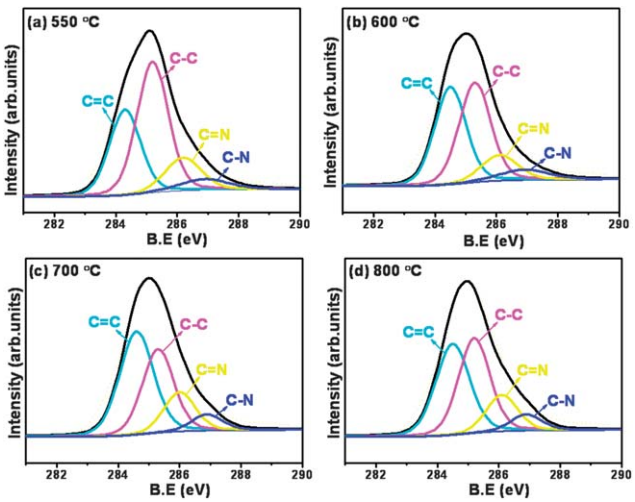

Fig. 3 C 1s XPS spectra of diamond nanowire films grown at 550–800 °C.

Table 2 The electrochemical parameters of diamond nanowire film electrodes obtained from voltammograms presented in Fig. S1†

Substrate temperature (T_S) (°C)	E_{pa} (mV)	E_{pc} (mV)	ΔE_p (mV)	I_{pa} (μA)	I_{pc} (μA)	I_{pa}/I_{pc} (μA)	Conductivity $(\Omega\ cm)^{-1}$	Active surface area (cm^2)
550	—	—	—	—	—	—	1.2	—
600	348	173	175	29.30	25.2	1.16	106	0.217
700	292	202	90	23.39	23.77	0.98	186	0.254
800	294	199	95	21.24	23.60	0.90	90	0.250
Graphite	315	105	210	46.70	42.12	1.10	185	0.132
BDD	259	161	98	47.57	57.67	0.82	106.9	0.202

C 1s core level line is composed of at least two components, with a higher binding shoulder (detected at 285.3 eV) as shown in Fig. 3. Therefore, the fitting of the DNW film C 1s peaks was performed by using Lorentzian peaks at binding energies of 284.3 eV and 285.3 eV which are attributed to the sp^2 C=C and sp^3 C–C bond atoms, respectively. The two peaks at 285.9 and 286.7 eV correspond to sp^2-hybridization bonding structures of C atoms bonded to N atoms (sp^2 C=N) and sp^3-hybridization bonding structures of C atoms bonded to N atoms (sp^3 C–N), respectively and their relative intensities are tabulated in Table 1. The background was detracted using Shirley's method. For the DNW films grown at 550 °C, sp^3 C–C bonding is predominant with a peak intensity of 48.1%, while sp^2 C=C intensity is 31.5%, whereas sp^2 C=N and sp^3 C–N appear with a peak intensity of 14.1 and 6.2%, respectively, The appearance of these two peaks indicates the formation of a chemical bond between C and N atoms after the incorporation of nitrogen. Upon increasing the T_S to 600 °C, the DNW film depicts an increase in the peak intensity of sp^2 C=C bonding with 40.1%, and a decrease in sp^3 C–C intensity with 41.0% as compared to 550 °C, whereas the sp^3 C–N and sp^2 C=N peak intensities are increased to 6.5 and 12.2%, respectively. On the other hand, 700 °C DNW film shows the lowest sp^3 C–C peak intensity of 33.4%, while sp^2 C=C displays 44.6% intensity. Incorporation of nitrogen results in two different N–C bonding state, including N–sp^3 C bond and N–sp^2 C bond. As the T_S increases to 700 °C, the N–sp^2 C bonds content increases, whereas, the N–sp^3 C bonds content decreases. Among all DNWs, the highest sp^2 C=N peak intensity of 15.5% was observed at 700 °C with sp^3 C–N bond intensity of 6.3%. At higher T_S, 800 °C, DNW films, sp^3 C–C bonding is dominant with a peak intensity of 38.5%, while sp^2 C=C intensity is 40.1%. From these data, it is clear that the sample grown at 700 °C possesses larger nitrogen incorporation, which enhances the EC behavior due to the larger sp^2 C=C bond intensity.

Fig. 4 shows a series of cyclic voltammetric (CV) *i–E* curves in 0.1 M PBS (pH 7.4) for DNW films at different T_S. It is clear that the responses between −2.5 V to 2.5 V (*vs.* Ag/AgCl) at a potential sweep rate 50 mV s^{-1} are similar, irrespective of the level of various T_S. The voltammograms cover a wide working potential window, a low voltammetric background current with the calculated potential range of ∼ >3.0 V of all DNW electrodes (Fig. 4), which are moderately larger than the graphite electrode (*ca.* 2.5 V).[79,80] These DNW electrodes are consistent with the cycle number which indicates that the surface structure is

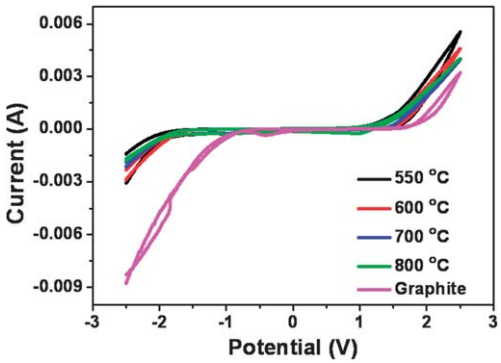

Fig. 4 Cyclic voltammogram (CV) curves at diamond nanowire film electrodes (550–800 °C) in 0.1 M PBS (pH 7.4) at a scan rate of 50 mV s^{-1}.

stable. These unique properties could be used to investigate the redox kinetics in electroanalytical chemistry. In addition, the CV curves, represented in Fig. S1 (see ESI†) show symmetrical anodic and cathodic peaks associated with the oxidation and reduction of $Fe(CN)_6^{3-/4-}$, $Ru(NH_3)_6^{2+/3+}$, and a 4-*tert*-butylcatechol couple on the DNW electrodes–solution interface. The separation between the anodic and cathodic peaks (ΔE_p) indicates a degree of reversibility of EC reaction. Most frequently the EC properties of an electrode are studied using ferrocyanide–ferricyanide in aqueous solution. The EC parameters of DNW film electrodes obtained from CVs (Fig. S1a†) show a quasi-reversible response for $Fe(CN)_6^{3-/4-}$ of ΔE_p values of 175, 90, 95, 210, and 98 mV for 600, 700 and 800 °C, graphite and BDD electrodes, respectively, and are summarized in Table 2. As expected, the sample grown at 550 °C did not show any redox activity, since the amorphous carbons were not electrochemically active and the redox process cannot be initiated.[81] At higher ΔE_p, the reaction becomes irreversible. A better peak separation is observed for all DNW film electrodes with a smaller ΔE_p value than for the graphite electrode ($\Delta E_p = 210$). The ratio of anodic to cathodic current peak, (I_{pa}/I_{pc}) is close to 1.0, indicating that $[Fe(CN)_6]^{3-/4-}$ redox reaction on these DNW film electrode is quasi-reversible and is not complicated by the other side reactions. Better peak separation is observed for DNW film electrodes than for the graphite electrode ($\Delta E_p = 210$) with the smaller ΔE_p value. Furthermore, a more reversible response is observed for $Ru(NH_3)_6^{2+/3+}$ with a ΔE_p value of 106 to 141 mV for 700 and 800 °C, respectively, is shown in Fig. S1b† which is comparable with the BDD electrode, indicating that the

Table 1 Relative intensities of various components of C 1s XPS spectra from N_2-incorporated diamond nanowire films grown at 550–800 °C

	Chemical bonding (%)			
DNW films grown at different substrate temperatures (T_S) (°C)	sp^2 C=C (284.5)	sp^3 C–C (285.3)	sp^2 C=N (285.9)	sp^3 C–N (286.7)
550	31.5	48.1	14.1	6.2
600	40.1	41.0	12.2	6.5
700	44.6	33.4	15.5	6.3
800	40.1	38.5	14.7	6.4

density of states and surface charge carrier concentration are sufficient at these potentials to support quasi-reversible electron transfer kinetics. In contrast to the other two redox analytes, a highly irreversible voltammetric *i–E* curve is observed for 4-*tert*-butylcatechol, as shown in Fig. S1c.† The larger ΔE_p value of DNW film electrodes (288 and 278 mV for the appropriate 700 and 800 °C electrodes) clearly demonstrates that the reaction is more irreversible. From the earlier reports,[82–84] it was depicted that the relatively slow electrode reaction kinetics had routinely been observed for microcrystalline and single crystal diamond using catechols and catecholamines.[85–87] Thus, the kinetics of this system can be influenced favorably by surface adsorption sites (*i.e.*, edge plane sites) and by carbon–nitrogen functionalities terminating the exposed edges of sp^2 carbon.[88] Based on the responses for the redox systems, we conclude that DNW film electrodes exhibit a high degree of EC activity without any conventional surface treatment over a potential range from 2.5 to −2.5 V (*vs.* Ag/AgCl). Since diamond is inherently a wide bandgap semiconductor, we suppose that the charge carriers within the DNW film electrodes result from sp^2 carbon phases residing in the grain boundaries.

Moreover, CVs based on ferricyanide redox reactions performed with varying scan rates are often used to estimate the active surface areas for electrodes by using the Randles-Sevcik equation ($I_p = 2.69 \times 10^5 AD_o^{1/2} n^{3/2} C_o v^{1/2}$).[89] Here, I_p is the reduction peak current in mA, A is the electrode ASA in cm^2, D_o is the diffusion coefficient of ferricyanide (7.01×10^{-6} cm^2 s^{-1}),[90] n is the number of electrons transferred in the reaction equation, C_o is the concentration of ferricyanide in M, and v is the scan rate in V s^{-1}. The calculated active surface areas of the electrodes are shown in Table 2. These results indicate that there is a significant increase from the geometric area (0.186 cm^2) of each DNW film electrodes. From these observations, it is clearly confirmed that the formation of a DNW-like film structure can be employed for EC electrode applications due to its larger surface area and low charge transfer resistance, which opens the possibility of an entire series of biosensor applications.

As stated earlier, we focused on the development of a detection scheme for biosensor applications based on the DNW film electrodes. These electrodes were used to identify AA, DA and UA electrochemically using CV and DPV. Fig. 5 shows the CV of DNW film electrodes grown using various T_S produced when sensing 0.1 mM AA, DA, and UA. The results shown in Fig. 5 and Table S1 (see ESI†), show that a DNW film electrode grown at $T_S = 700$ °C outperforms all other DNW film electrode materials in terms of the peak currents in the CV curves. For the detection of AA, the peak current of each DNW film electrodes varied from 1.9–29.8 μA. Among these electrodes, the DNW film (700 °C) electrode in Fig. 5b can reach 29.8 μA with a lower peak potential than that of the other materials, indicating better peak separation. For the detection of DA and UA, the peak currents varied from 50.6–90.9 μA to 7.6–91.6 μA respectively, with respect to T_S. Among all DNW film electrodes, the DNW film (700 °C) electrode in Fig. 5a and c shows 90.9 and 91.6 μA peak current, respectively, which is larger than that of the DNW film grown at low T_S (500 °C). Thus, it has been found that DNW film electrodes provide an increase in EC characteristic with respect to the T_S. A substantial body of literature[61–66] also accepts that the nitrogen incorporation in diamond films can cause defects and the creation of sp^2 carbon in the grain boundaries. Therefore, it was suggested that many dangling bonds present in the grain boundaries of these DNW film electrodes are responsible for the enhanced EC sensing.

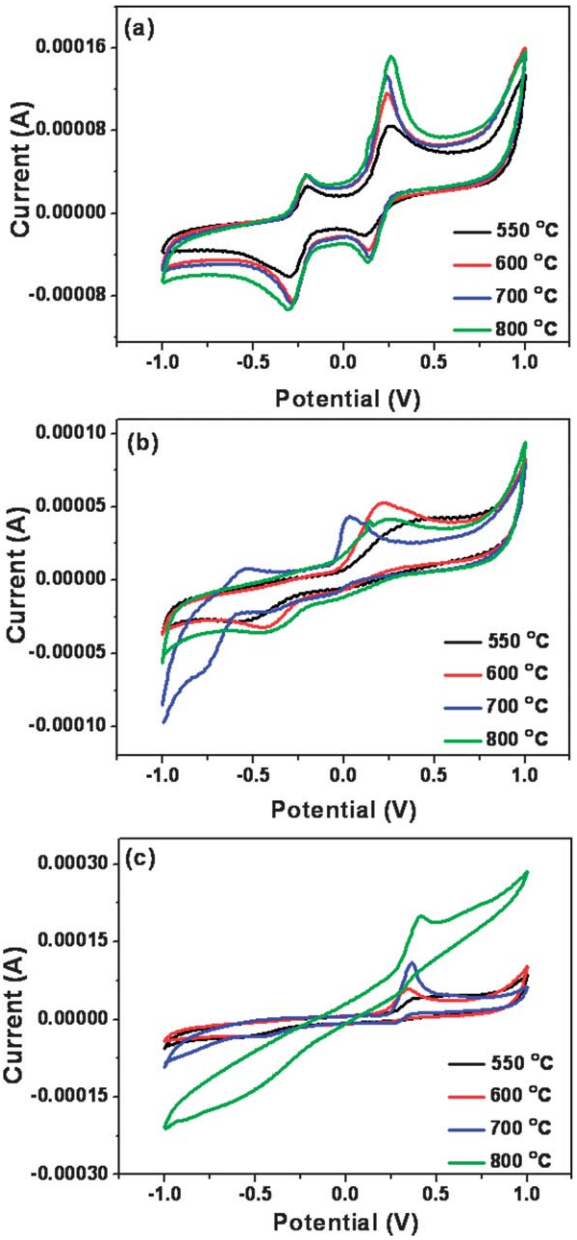

Fig. 5 (a, b and c) Cyclic voltammetric *i–E* curves of DNW film electrodes at T_S (no iR correction) for the redox analytes: (a) 0.1 mM DA, (b) 0.1 mM AA and (c) 0.1 mM UA in 0.1 M PBS (pH 7.4).

Furthermore, the interference of AA is a major problem during the EC determination of biological substrates such as dopamine.[91] Previous reports illustrate that the bare electrode surface should be modified carefully with selected mediators, to reduce or prevent the possibility of electrode fouling.[92,93] Due to

the higher sensitivity of pulse techniques, DPV was used to further investigate the interference between AA, DA and UA were studied by using DNW film electrodes in a solution containing a mixture of three analytes. Fig. 6 shows the DPV curves of DNW film electrodes in a solution of 0.33 mM AA + 0.033 mM DA + 0.033 mM UA. The peak potentials at +0.0 V, +0.15 V and 0.28 V are due to the electro-oxidation of AA, DA and UA, respectively. The voltammetric peak separations of AA–DA, DA–UA, and AA–UA, are shown in Fig. 6, which indicates that the DNW (700 °C) is highly sensitive towards the DA detection in the solution mixture. Among all DNW film electrodes, the DNW film grown at T_S = 700 °C shows better peak separation (148.5, 138, 286.1 mV for AA–DA, DA–UA and AA–UA respectively) between the aforementioned analytes, which is comparable to graphene/Pt GC[88] and GONR (200 W)/GCE[94] electrode materials. In addition, the DPV results shown in Fig. S2 (see ESI†) clearly reveals that DNW film electrode has a far better performance, whereas the peak separation of AA–DA, DA–UA and AA–UA has not been well resolved at the BDD electrode due to oxidation of AA at a lower degree of EC reversibility. Similar results were observed for other bare electrodes such as graphite and glassy carbon which lacks in sensitivity. The amperometric responses of the DNW film electrodes to DA are depicted in Fig. 7, showing a typical amperogram of DNW film electrodes obtained by the addition of different DA concentrated analyte solutions in a stirred 0.1 M phosphate buffer solution (PBS, pH 7.4). We monitored the oxidation current of a specific analyte at a fixed potential of +0.2 V. Fig. 7c shows a typical amperogram of DNW film (700 °C) electrode obtained at a potential of +0.2 V for different DA concentrations.

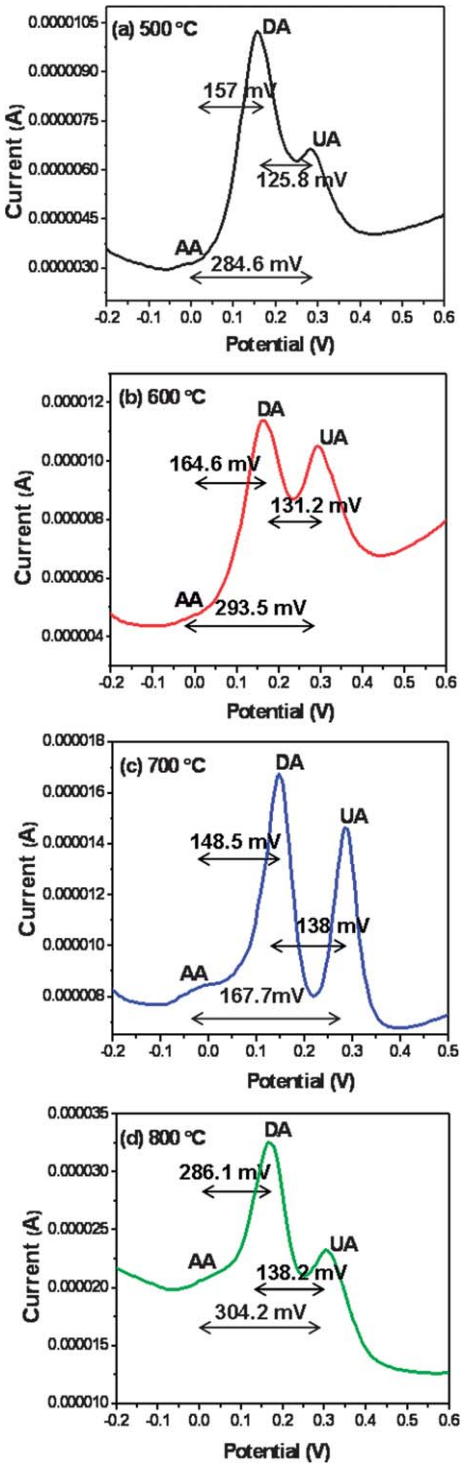

Fig. 6 (a, b, c and d) Differential pulse voltammetry curves for DNW film electrodes at T_S in a solution containing 0.33 mM AA + 0.033 mM DA + 0.033 mM UA.

The corresponding plots of the currents with respect to the analyte concentrations are plotted in Fig. 8. A linear relationship between the current and the concentration of DA was obtained for the concentration range of 0.5 to 10 μM, shown as inset in Fig. 8 (blue line). The linear regression equation is $I_{DA} = 0.1279C_{DA} + 0.0002$, with a correlation coefficient of $r = 0.9958$ ($N = 3$). The detection limit for DA was found to be 0.36 μM. The analytical parameters for the DNW 700 °C in Fig. 7c are summarized in Table 3. In Tables S2 and S3,† the data obtained from using DNW film (700 °C) electrode for detection of DA, AA and UA by *i*–*t* measurements and CV were compared with those using other electrodes found in the literature. The DNW film (700 °C) electrode was further used to detect DA at a range of concentrations (0.0006–0.06 mM DA) in the presence of 0.6 mM AA using DPV (figure not shown). The oxidation current of DA increases with an increase of DA concentration. However, the concentration of DA is greater than 50 μM, and the oxidation current increases slowly. In contrast, the DA oxidation current is linearly proportional to its concentration in the low concentration range, from 0.5 to 10 μM, shown in the inset of Fig. 8 (red line) and the linear regression equations $I_{DA} = 0.1907 + 0.0026C_{DA}$, with a correlation coefficient of $r = 0.9657$ ($N = 3$), the slope corresponds to the sensitivity of the DNW film (700 °C) electrode for detection of DA in the presence of AA and UA. The dynamic range and detection limit using DNW film (700 °C) electrode without surface modification are comparable to those of other modified electrodes like BDD, graphite, nanocarbon modified GC electrodes found in the literature (Table S4).† The enhancement in the EC behavior of DNW film electrode is probably due to presence of graphitic carbon, which is confirmed by the NEXAFS (Fig. 2) and XPS (Fig. 3) respectively. The presence of graphitic carbon in all DNW film electrodes provides strong evidence for the existence of a sp^2 carbon

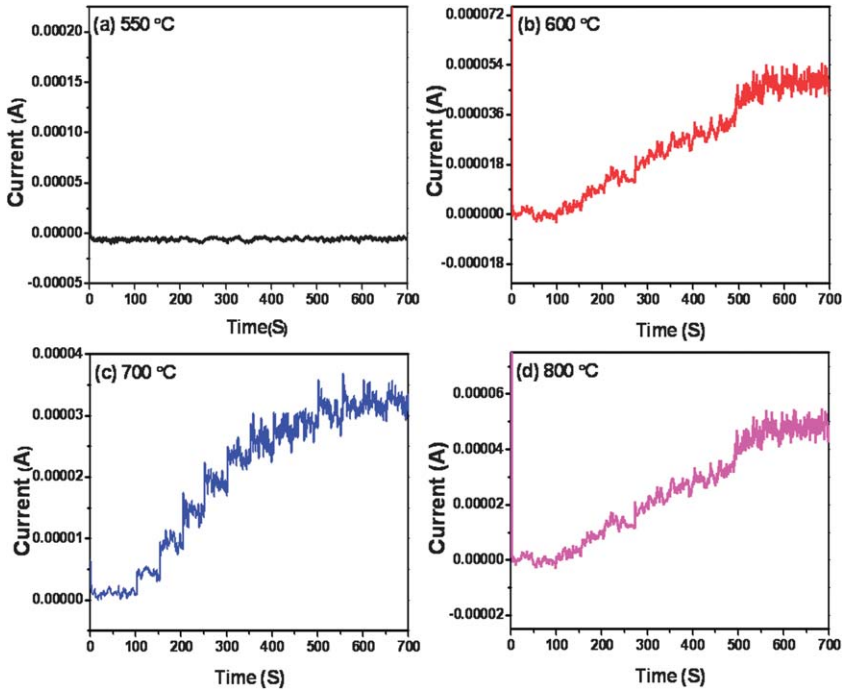

Fig. 7 Amperometric responses of DA for DNW film electrodes without any additional surface modification (a) 550 °C, (b) 600 °C, (c) 700 °C and (d) 800 °C in a 0.1 M PBS solution.

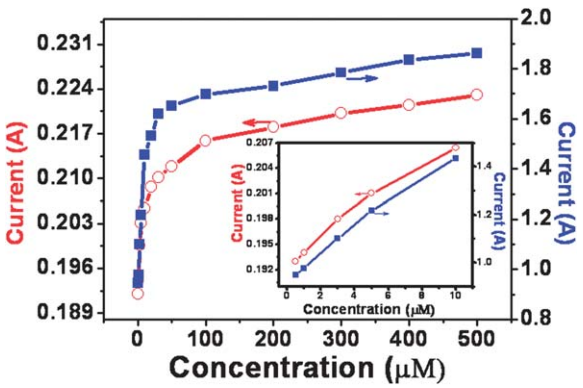

Fig. 8 Plot of the oxidation current of DA (I_{DA}) *vs.* the concentration (C_{DA}) for the amperometric method (blue line) and DPV (red line) in the presence of AA. Inset shows a low range linear calibration curve. Here, the electrode used is DNW film grown at 700 °C.

network. Such nanowire-like morphology has significant implications on the outstanding electrochemical performance for the *in situ* detection of DA in the ternary mixture.

Conclusion

This work demonstrates the fabrication of N_2-incorporated DNW films using MPECVD and used for the simultaneous detection of AA, DA, and UA. The N_2-incorporated DNW film electrodes show excellent electrocatalytic activity towards the oxidation of small molecules, such as AA, DA, and UA. The detection limit and potential shifts values obtained by these electrodes are comparable with other modified electrodes like BDD, graphite, nanocarbon modified GC electrodes (Table S4).† The EC behavior of N_2-incorporated conducting DNW films has been studied by CV and DPV in both the absence and presence of AA and UA. The results of DPV show that N_2-incorporated DNW electrodes exhibit highly electro catalytic activity to the oxidations of AA and UA. High selectivity and reliable anti-fouling ability may promote the DNW film electrodes to be an effective sensor for direct determination of AA, DA, and UA in a real sample. The presence of sp^2 graphitic phase and the nanowire-like structure could be responsible for outstanding EC properties, and exhibits a considerable degree of potential on the bio-sensing platform. We believe that the DNW film

Table 3 Analytical parameters for the amperometric determination of DA using DNW film (700 °C) electrode without any surface modification

Electrode	Linear range (μmol L^{-1})	Linear regression equation I_{pa} (μA), C (μmol L^{-1})	Correlation coefficient (r)	Limit of detection (LOD) (μmol L^{-1})		Sensitivity (μA μM^{-1})
				Exp.	Cal.	
DNW film (700 °C)	0.5–500	$I_{DA} = 0.1279C_{DA} + 0.0002$	0.9928	0.5	0.36	0.1226

electrodes can play a significant role in sensing the DA in real samples like blood, serum and plasma.

Notes

The authors declare no competing financial interest.

Acknowledgements

We thank the National Science Council for financial support under NSC 99-2119-M-032-003-MY2 and NSC 100-2113-M-007-006.

References

1 (*a*) M. A. T. Gilmartin and J. P. Hart, *Analyst*, 1995, **120**, 1029; (*b*) H. Remita, P. F. Siril, I. M. Mbomekalle, B. Keita and L. Nadjo, *J. Solid State Electrochem.*, 2005, **10**, 506.
2 G. Jin, Y. Zhang and W. Cheng, *Sens. Actuators, B*, 2005, **107**, 528.
3 P. Damier, E. C. Hirsch, Y. Agid and A. M. Graybiel, *Brain*, 1999, **122**, 1437.
4 S. Marceglia, G. Foffani, A. M. Bianchi, G. Baselli, F. Tamma, M. Egidi and A. Priori, *J. Physiol.*, 2006, **571**, 579.
5 L. Schwieler, G. Engberg and S. Erhardt, *Synapse*, 2004, **52**, 114.
6 G. Hu, D. Zhang, W. Wu and Z. Yang, *Colloids Surf., B*, 2008, **62**, 199.
7 H. Gu, Y. Xu, W. Peng, G. Li and H. Chen, *Microchim. Acta*, 2004, **146**, 223.
8 M. Ates, J. Castillo, A. S. Sarac and W. Schuhmann, *Microchim. Acta*, 2007, **160**, 247.
9 L. Zhang, *Microchim. Acta*, 2007, **161**, 191.
10 Y. Zhang, G. Jin, Z. Yang and H. Zhao, *Microchim. Acta*, 2004, **147**, 225.
11 G. S. Lai, H. L. Zhang and D. Y. Han, *Microchim. Acta*, 2007, **160**, 233.
12 K. Wu and S. Hu, *Microchim. Acta*, 2004, **144**, 131.
13 R. D. O'Neill, *Analyst*, 1994, **119**, 767.
14 I. Koshiishi and T. Imanari, *Anal. Chem.*, 1997, **69**, 216.
15 Z. Wang, Y. Wang and G. Luo, *Analyst*, 2002, **127**, 1353.
16 F. Gonon, M. Buda, R. Cespuglio, M. Jouvet and J. F. Pujol, *Nature*, 1980, **286**, 902.
17 A. Salimi, H. Mam-Khezri and R. Hallaj, *Talanta*, 2006, **708**, 23.
18 P. Shakkthivel and S. M. Chen, *Biosens. Bioelectron.*, 2007, **22**, 1680.
19 S. Shahrokhian and H. R. Zare-Mehrjardi, *Sens. Actuators, B*, 2007, **121**, 530.
20 S. Thiagarajan and S. M. Chen, *Talanta*, 2007, **74**, 212.
21 C. R. Raj, T. Okajima and T. Ohsaka, *J. Electroanal. Chem.*, 2003, **543**, 127.
22 M. Behpour, S. M. Ghoreishi, E. Honarmand and M. S. Niasari, *Analyst*, 2011, **136**, 1979.
23 J. Chen, J. Zhang, X. Lin, H. Wan and S. Zhang, *Electroanalysis*, 2007, **19**, 612.
24 N. Chauhan, J. Narang and C. S. Pundir, *Analyst*, 2011, **136**, 1938.
25 J. Breczko, M. E. Plonska-Brzezinska and L. Echegoyen, *Electrochim. Acta*, 2012, **72**, 61.
26 Q. Xu, L. L. Chen, G. J. Lu, X. Y. Hu, H. B. Li, L. L. Ding and Y. Wang, *J. Appl. Electrochem.*, 2010, **41**, 143.
27 W. Ren, H. Q. Luo and N. B. Li, *Biosens. Bioelectron.*, 2006, **21**, 1086.
28 R. P. D. Silva, A. W. O. Lima and S. H. P. Serrano, *Anal. Chim. Acta*, 2008, **612**, 89.
29 Z. Wang, J. Liu, Q. Liang, Y. Wang and G. Luo, *Analyst*, 2002, **127**, 653.
30 A. Salimi, H. MamKhezri and R. Hallaj, *Talanta*, 2006, **70**, 823.
31 N. Jia, Z. Wang, G. Yang, H. Shen and L. Zhu, *Electrochem. Commun.*, 2007, **9**, 233.
32 R. T. Kachoosangi and R. G. Compton, *Anal. Bioanal. Chem.*, 2007, **387**, 2793.
33 K. S. Prasad, G. Muthuraman and J. M. Zen, *Electrochem. Commun.*, 2008, **10**, 559.
34 G. Liu, J. Li, L. Wang, N. Zong, S. Yu and F. Li, *Anal. Methods*, 2012, **4**, 609.
35 C. Y. Liu, L. Z. Yang, F. Song, L. Y. Jiang and G. H. Lu, *Chin. Chem. Lett.*, 2005, **16**, 237.
36 S. Raina, W. P. Kang and J. L. Davidson, *Diamond Relat. Mater.*, 2008, **17**, 896.
37 J. B. Posthill, D. P. Malta, T. P. Humphreys, G. C. Hudson, R. E. Thomas, R. A. Rudder and R. J. Markunas, *J. Appl. Phys.*, 1996, **79**, 2722.
38 J. Isberg, J. Hammersberg, E. Johnannson, T. Wilkstrom, D. J. Twitchen, A. J. Whitehead, S. E. Coe and G. A. Scarsbrook, *Science*, 2002, **297**, 1670.
39 R. Torz-Piotrowska, A. Wrzyszczyński, K. Paprocki, M. Szreiber, C. Uniszkiewicz and E. Staryga, *J. Achieve. Mater. Manuf. Eng*, 2009, **37**, 486.
40 P. Actis, A. Denoyelle, R. Boukherroub and S. Szunerits, *Electrochem. Commun.*, 2008, **10**, 402.
41 B. J. Venton and R. M. Wightman, *Anal. Chem.*, 2003, **75**, 414A.
42 R. M. Wightman, L. J. May and A. C. Michael, *Anal. Chem.*, 1988, **60**, 769A.
43 J. A. Stamfold and J. B. Justice, Jr, *Anal. Chem.*, 1996, **68**, 359A.
44 A. Sakharova, L. Nyikos and Y. Pleskov, *Electrochim. Acta*, 1992, **37**, 973.
45 K. Patel, K. Hashimoto and A. Fujishima, *J. Photochem. Photobiol., A*, 1992, **65**, 419.
46 R. Tenne, K. Patel, K. Hashimoto and A. Fujishima, *J. Electroanal. Chem.*, 1993, **347**, 409.
47 G. M. Swain and R. Ramesham, *Anal. Chem.*, 1993, **65**, 345.
48 E. Popa, H. Notsu, T. Miwa, D. A. Tryk and A. Fujishima, *Electrochem. Solid-State Lett.*, 1999, **2**, 49.
49 D. A. Tryk, H. Tachibana, H. Inoue and A. Fujishima, *Diamond Relat. Mater.*, 2007, **16**, 881.
50 E. Popa, Y. Kubota, D. A. Tryk and A. Fujishima, *Anal. Chem.*, 2000, **72**, 1724.
51 Y. Zhou and J. F. Zhi, *Electrochem. Commun.*, 2006, **8**, 1811.

52 Y. L. Zhou, R. H. Tian and J. F. Zhi, *Biosens. Bioelectron.*, 2007, **22**, 822.
53 J. Weng, J. Xue, J. Wang, J. Ye, H. Cui, F. Sheu and Q. Zhang, *Adv. Funct. Mater.*, 2005, **15**, 639.
54 C. Terashima, T. N. Rao, B. V. Sarada and A. Fujishima, *Chem. Lett.*, 2003, **32**, 136.
55 T. A. Ivandini, K. Honda, T. N. Rao, A. Fujishima and Y. Einaga, *Talanta*, 2007, **71**, 648.
56 N. Spataru, B. V. Sarada, E. Popa, D. A. Tryk and A. Fujishima, *Anal. Chem.*, 2001, **73**, 514.
57 J. C. Harfield, K. E. Toghill, C. Batchelor-Mcauley, C. Downing and R. G. Compton, *Electroanalysis*, 2011, **23**, 931.
58 S. Bhattacharyya, *Phys. Rev. B: Condens. Matter Mater. Phys.*, 2004, **70**, 125412.
59 (*a*) K. J. Sankaran, P. T. Joseph, N. H. Tai and I. N. Lin, *Diamond Relat. Mater.*, 2010, **19**, 927; (*b*) K. J. Sankaran, J. Kurian, H. C. Chen, C. L. Dong, C. Y. Lee, N. H. Tai and I. N. Lin, *J. Phys. D: Appl. Phys.*, 2012, **45**, 365303.
60 C. R. Lin, W. H. Liao, D. H. Wei, J. S. Tsai, C. K. Chang and W. C. Fang, *Diamond Relat. Mater.*, 2011, **20**, 380.
61 D. Zhou, A. R. Krauss, L. C. Qin, T. G. McCauley, D. M. Gruen, T. D. Corrigan, R. P. H. Chan and H. Gnaser, *J. Appl. Phys.*, 1997, **82**, 4546.
62 J. Birrell, J. E. Gerbi, O. Auciello, J. M. Gibson, D. M. Gruen and J. A. Carlisle, *J. Appl. Phys.*, 2003, **93**, 5606.
63 Y. C. Chen, N. H. Tai and I. N. Lin, *Diamond Relat. Mater.*, 2008, **17**, 457.
64 J. S. Tsai, C. K. Chang and W. C. Fang, *Diamond Relat. Mater.*, 2011, **20**, 380.
65 R. Arenal, P. Bruno, D. J. Miller, M. Bleuel, J. Lal and D. M. Gruen, *Phys. Rev. B: Condens. Matter Mater. Phys.*, 2007, **75**, 195431.
66 A. R. Sobia, S. Adnan, A. Mukhtiar, A. A. Khurram, A. A. Turab, A. Awaisa, A. Naveed, Q. J. Faisal, H. Javaid and G. Yu, *Curr. Appl. Phys.*, 2012, **12**, 712.
67 S. A. Rakha, G. Yu, J. Cao, S. He and X. Zhou, *J. Appl. Phys.*, 2010, **107**, 114324.
68 K. Teii and T. Ikeda, *Diamond Relat. Mater.*, 2007, **16**, 753.
69 S. Raina, W. P. Kang and J. L. Davidson, *Diamond Relat. Mater.*, 2009, **18**, 574.
70 S. Raina, W. P. Kang and J. L. Davidson, *Diamond Relat. Mater.*, 2009, **18**, 718.
71 S. Raina, W. P. Kang and J. L. Davidson, *Diamond Relat. Mater.*, 2010, **19**, 256.
72 J. Birrell, J. E. Gerbi, O. Auciello, J. M. Gibson, D. M. Gruen and J. A. Carlisle, *J. Appl. Phys.*, 2003, **93**, 5606.
73 X. Xiao, J. Birrell, J. E. Gerbi, O. Auciello and J. A. Carlisle, *J. Appl. Phys.*, 2004, **96**, 2232.
74 P. T. Joseph, N. H. Tai, C. H. Chen, H. Niu, H. F. Cheng, W. F. Pong and I. N. Lin, *J. Phys. D: Appl. Phys.*, 2009, **42**, 105403.
75 F. L. Coffman, R. Cao, P. A. Pianetta, S. Kapoor, M. Kelly and L. Terminello, *Appl. Phys. Lett.*, 1996, **69**, 568.
76 C. R. Lin, W. H. Liao, D. H. Wei, C. K. Chang, W. C. Fang, C. L. Chen, C. L. Dong, J. L. Chen and J. H. Guo, *J. Cryst. Growth*, 2011, **326**, 212.
77 Y. K. Chang, H. H. Hsieh, W. F. Pong, M. H. Tsai, F. Z. Chien, P. K. Tseng, L. C. Chen, T. Y. Wang, K. H. Chen, D. M. Bhusari, J. R. Yang and S. T. Lin, *Phys. Rev. Lett.*, 1999, **82**, 5377.
78 N. Shang, P. Papakonstantinou, P. Wang, A. Zakharov, U. Palnitkar, I. N. Lin, M. Chu and A. Stamboulis, *ACS Nano*, 2009, **3**, 1032.
79 R. L. Mc. Creery, *Chem. Rev.*, 2008, **108**, 2646.
80 (*a*) Y. V. Pleskov, *Russ. J. Electrochem.*, 2002, **38**, 1275; (*b*) R. Ramesham and M. F. Rose, *Diamond Relat. Mater.*, 1997, **6**, 17.
81 Y. V. Pleskov, M. D. Krotowa, V. I. Polyakov, A. V. Khomich, A. J. Rukovischuikov, B. L. Druz and I. Zaritsky, *J. Electroanal. Chem.*, 2002, **519**, 60.
82 B. Fausett, M. C. Granger, M. L. Hupert, J. Wang, G. M. Swain and D. M. Gruen, *Electroanalysis*, 2000, **12**, 7.
83 J. Xu, M. C. Granger, Q. Chen, T. E. Lister, J. W. Strojek and G. M. Swain, *Anal. Chem.*, 1997, **69**, 591A.
84 G. M. Swain, A. B. Anderson and J. C. Angus, *MRS Bull.*, 1998, **23**, 56.
85 K. R. Kneten and R. L. McCreery, *Anal. Chem.*, 1992, **64**, 2518.
86 S. Alehashem, F. Chambers, J. W. Strojek, G. M. Swain and R. Ramesham, *Anal. Chem.*, 1995, **67**, 2812.
87 J. O. Howell, W. G. Kuhr, R. E. Ensman and R. M. Wightman, *J. Electroanal. Chem.*, 1986, **209**, 77.
88 K. R. Kneten and R. L. McCreery, *Anal. Chem.*, 1992, **64**, 2518.
89 W. Ostwald, *Lehrbuch der Allgemeinen Chemie*, W. Engelmann: Leipzig, Germany, 1887.
90 *Electrochemical Methods: Fundamentals and Applications*, ed. A. J. Bard L. Faulkner, Wiley, New York, 2nd edn, 2001.
91 P. Actis, A. Denoyelle, R. Boukherroub and S. Szunerits, *Electrochem. Commun.*, 2008, **10**, 402.
92 J. Moiroux and P. J. Elving, *J. Am. Chem. Soc.*, 1980, **102**, 6533.
93 M. Musameh, J. Wang, A. Merkoci and Y. Lin, *Electrochem. Commun.*, 2002, **4**, 743.
94 C. L. Sun, C. T. Chang, H. H. Lee, J. Zhou, J. Wang, T. K. Sham and W. F. Pong, *ACS Nano*, 2011, **5**, 7788.